Inorg. Chem. **2007**, *46*, 7012–7023

New Luminescent Solids in the Ln–W(Mo)–Te–O–(Cl) Systems

Hai-Long Jiang,[†,‡] En Ma,[†] and Jiang-Gao Mao*[,†]

State Key Laboratory of Structural Chemistry, Fujian Institute of Research on the Structure of Matter, Chinese Academy of Sciences, Fuzhou 350002, People's Republic of China, and Graduate School of the Chinese Academy of Sciences, Beijing 100039, People's Republic of China

Received April 25, 2007

Solid-state reactions of lanthanide(III) oxide (and/or lanthanide(III) oxychloride), MoO_3 (or WO_3), and TeO_2 at high temperature lead to eight new luminescent compounds with four different types of structures, namely, $Ln_2(MoO_4)(Te_4O_{10})$ (Ln = Pr, Nd), $La_2(WO_4)(Te_3O_7)_2$, $Nd_2W_2Te_2O_{13}$, and $Ln_5(MO_4)(Te_5O_{13})(TeO_3)_2Cl_3$ (Ln = Pr, Nd; M = Mo, W). The structures of $Ln_2(MoO_4)(Te_4O_{10})$ (Ln = Pr, Nd) feature a 3D network in which the MoO_4 tetrahedra serve as bridges between two lanthanide(III) tellurite layers. $La_2(WO_4)(Te_3O_7)_2$ features a triple-layer structure built of a $[La_2WO_4]^{4+}$ layer sandwiched between two $Te_3O_7^{2-}$ anionic layers. The structure of $Nd_2W_2Te_2O_{13}$ is a 3D network in which the $W_2O_{10}^{8-}$ dimers were inserted in the large tunnels of the neodymium(III) tellurites. The structures of $Ln_5(MO_4)(Te_5O_{13})(TeO_3)_2Cl_3$ (Ln = Pr, Nd; M = Mo, W) feature a 3D network structure built of lanthanide(III) ions interconnected by bridging TeO_3^{2-}, $Te_5O_{13}^{6-}$, and Cl^- anions with the MO_4 (M = Mo, W) tetrahedra capping on both sides of the Ln_4 (Ln = Pr, Nd) clusters and the isolated Cl^- anions occupying the large apertures of the structure. Luminescent studies indicate that $Pr_2(MoO_4)(Te_4O_{10})$ and $Pr_5(MO_4)(Te_5O_{13})(TeO_3)_2Cl_3$ (M = Mo, W) are able to emit blue, green, and red light, whereas $Nd_2(MoO_4)(Te_4O_{10})$, $Nd_2W_2Te_2O_{13}$, and $Nd_5(MO_4)(Te_5O_{13})(TeO_3)_2Cl_3$ (M = Mo, W) exhibit strong emission bands in the near-IR region.

Introduction

Metal selenites and tellurites can form a variety of unusual structures as a result of the presence of the stereochemically active lone-pair electrons, which may serve as an invisible structure-directing agent.[1] The structures of metal tellurites display much more diversity than the corresponding selenites because the TeO_x (x = 3, 4, 5) groups could be further interconnected into a variety of polymeric tellurium(IV) oxide anions with extended structures.[2,3] The asymmetric coordination polyhedron adopted by a Se(IV) or Te(IV) atom may also result in noncentrosymmetric structures with possible second harmonic generation properties.[4–6] Transition-metal ions susceptible to second-order Jahn−Teller distortions have also been introduced to the metal selenite or tellurite systems to reinforce the polarization of these structures.[4–6] Although a number of lanthanide selenites and tellurium(IV) oxides have been reported,[1,7,8] reports on

* To whom correspondence should be addressed. E-mail: mjg@fjirsm.ac.cn.
† Chinese Academy of Sciences.
‡ Graduate School of the Chinese Academy of Sciences.

(1) (a) Wickleder, M. S. *Chem. Rev.* **2002**, *102*, 2011 and references cited therein. (b) Verma, V. P. *Thermochim. Acta* **1999**, *327*, 63 and references cited therein.
(2) (a) Nikiforov, G. B.; Kusainova, A. M.; Berdonosov, P. S.; Dolgikh, V. A.; Lightfoot, P. *J. Solid State Chem.* **1999**, *146*, 473. (b) Meier, S. F.; Schleid, T. *Z. Anorg. Allg. Chem.* **2003**, *629*, 1575.
(3) (a) Ok, K. M.; Halasyamani, P. S. *Chem. Mater.* **2001**, *13*, 4278. (b) Halasyamani, P. S. *Chem. Mater.* **2004**, *16*, 3586.
(4) (a) Ra, H. S.; Ok, K. M.; Halasyamani, P. S. *J. Am. Chem. Soc.* **2003**, *125*, 7764. (b) Goodey, J.; Ok, K. M.; Broussard, J.; Hofmann, C.; Escobedo, F. V.; Halasyamani, P. S. *J. Solid State Chem.* **2003**, *175*, 3. (c) Ok, K. M.; Halasyamani, P. S. *Inorg. Chem.* **2004**, *43*, 4248. (d) Ok, K. M.; Orzechowski, J.; Halasyamani, P. S. *Inorg. Chem.* **2004**, *43*, 964.
(5) (a) Hart, R. T.; Ok, K. M.; Halasyamani, P. S.; Zwanziger, J. W. *Appl. Phys. Lett.* **2004**, *85*, 938. (b) Porter, Y.; Halasyamani, P. S. *J. Solid State Chem.* **2003**, *174*, 441. (c) Goodey, J.; Broussard, J.; Halasyamani, P. S. *Chem. Mater.* **2002**, *14*, 3174.
(6) (a) Harrison, W. T. A.; Dussack, L. L.; Jacobson, A. J. *J. Solid. State Chem.* **1996**, *125*, 234. (b) Johnston, M. G.; Harrison, W. T. A. *Inorg. Chem.* **2001**, *40*, 6518. (c) Balraj, V.; Vidyasagar, K. *Inorg. Chem.* **1999**, *38*, 5809. (d) Balraj, V.; Vidyasagar, K. *Inorg. Chem.* **1999**, *38*, 3458.
(7) (a) Wontcheu, J.; Schleid, T. *J. Solid State Chem.* **2003**, *171*, 429. (b) Wontcheu, J.; Schleid, T. *Z. Anorg. Allg. Chem.* **2002**, *628*, 1941. (c) Ruck, M.; Schmidt, P. *Z. Anorg. Allg. Chem.* **2003**, *629*, 2133. (d) Wontcheu, J.; Schleid, T. *Z. Anorg. Allg. Chem.* **2003**, *629*, 1463. (e) Krugermann, I.; Wickleder, M. S. *J. Solid State Chem.* **2002**, *167*, 113. (f) Krugermann, I.; Wickleder, M. S. *Z. Anorg. Allg. Chem.* **2002**, *628*, 147.
(8) (a) Ljjaali, I.; Flaschenrien, C.; Ibers, J. A. *J. Alloys Compd.* **2003**, *354*, 115. (b) Weber, F. A.; Meier, S. F.; Schleid, T. *Z. Anorg. Allg. Chem.* **2001**, *627*, 2225. (c) Meier, S. F.; Weber, F. A.; Glaser, R. J.; Schleid, T. *Z. Anorg. Allg. Chem.* **2001**, *627*, 2448. (d) Shen, Y. L.; Mao, J. G. *J. Alloys Compd.* **2004**, *385*, 86.

10.1021/ic700793n CCC: $37.00
Published on Web 07/11/2007

lanthanide selenites or tellurium(IV) oxides with transition-metal ions are still relatively rare.[1,9] Lanthanide compounds such as Er(III) and Nd(III) compounds exhibit good luminescent properties in the near-IR region, which have important applications such as optical signal amplifiers and lasers.[10] It is assumed that the use of two types of anions (SeO_3^{2-} or TeO_3^{2-} anion and molybdate or tungstate) for activating the lanthanide(III) ions can improve their luminescent properties. On the basis of this assumption, four lanthanide selenites or tellurites decorated by MoO_4 or MoO_6 polyhedra, namely, $Nd_2MoSe_2O_{10}$, $Gd_2MoSe_3O_{12}$, $La_2MoTe_3O_{12}$, and $Nd_2MoTe_3O_{12}$, were reported by our group recently.[11] It is noted that the tellurites normally adopt structures different from the corresponding selenites and the lanthanide contraction also plays an important role in the structures of the compounds formed.[11] W(VI) and V(V) elements could display a coordination geometry similar to that of Mo(VI); hence, it is anticipated that a variety of new compounds can be discovered in the Ln−W(V)−Se(Te)−O systems. The introduction of a halide anion into the above systems may also help in the formation of new compounds with interesting luminescent properties. Our research efforts to explore new compounds in the Ln−Mo(W)−Se(Te)−O(−Cl) systems afforded eight new lanthanide tellurium oxides (or oxychlorides) containing MoO_4/WO_4 tetrahedra or WO_6 octahedra, namely, $Ln_2(MoO_4)(Te_4O_{10})$ (Ln = Pr, Nd), $La_2(WO_4)(Te_3O_7)_2$, $Nd_2W_2Te_2O_{13}$, and $Ln_5(MO_4)(Te_5O_{13})(TeO_3)_2Cl_3$ (Ln = Pr, Nd; M = Mo, W). These compounds display four new structural types and interesting luminescent properties. Herein we report their syntheses, crystal structures, and luminescent properties.

Experimental Section

Materials and Instrumentation. All of the chemicals except LnOCl (Ln = Pr, Nd) were analytically pure from commercial sources and were used without further purification. Transition-metal or lanthanide oxides were purchased from the Shanghai Reagent Factory, and TeO_2 (99+%) was purchased from Acros Organics. LnOCl (Ln = Pr, Nd) were synthesized by heating the corresponding $LnCl_3 \cdot nH_2O$ (Ln = Pr, Nd) in air at 400 °C for 12 h.[12] Chemical compositions of all of the compounds were studied by a field emission scanning electron microscope (JSM6700F) equipped with an energy-dispersive X-ray spectroscope (EDS, Oxford INCA). Powder X-ray diffraction (XRD) patterns were collected on an XPERT-MPD $\theta-2\theta$ diffractometer. IR spectra were recorded on a Magna 750 FTIR spectrometer as KBr pellets in the range of 4000−400 cm^{-1}. Thermogravimetric analyses (TGA) were carried out with a NETZSCH STA 449C unit at a heating rate of 10 °C/min under an oxygen atmosphere. Room-temperature solid-state luminescent studies of $Pr_2(MoO_4)(Te_4O_{10})$, $La_2(WO_4)(Te_3O_7)_2$, and $Pr_5(MO_4)(Te_5O_{13})(TeO_3)_2Cl_3$ (M = Mo, W) were performed on a JY FluoroMax-3 spectrophotometer at room temperature with a wavelength increment of 1.0 nm and an integration time of 0.1 s. Room temperature luminescent properties of $Nd_2(MoO_4)(Te_4O_{10})$, $Nd_2W_2Te_2O_{13}$, and $Nd_5(MO_4)(Te_5O_{13})(TeO_3)_2Cl_3$ (M = Mo, W) were performed on an Edinburgh FLS920 fluorescence spectrometer with a microsecond flash lamp (μF900, Edinburgh) as the excitation source (resolution 1.0 nm). Low-temperature luminescent properties of $Nd_2(MoO_4)(Te_4O_{10})$ and $Nd_2W_2Te_2O_{13}$ were also performed on the Edinburgh FLS920 fluorescence spectrometer with a resolution of 0.15 nm. Magnetic susceptibility measurements on polycrystalline samples were performed with a PPMS-9T magnetometer at a field of 5000 Oe in the range of 2−300 K.

Preparation of $Ln_2(MoO_4)(Te_4O_{10})$ (Ln = Pr, Nd). Single crystals of $Pr_2(MoO_4)(Te_4O_{10})$ (prismatic in shape and light green in color) were obtained together with some other unidentified powders by the solid-state reaction of a mixture containing Pr_2O_3 (0.083 g, 0.25 mmol), MoO_3 (0.036 g, 0.25 mmol), and TeO_2 (0.240 g, 1.5 mmol) in an evacuated quartz tube at 750 °C for 6 days and then slowly cooled to 350 °C at a cooling rate of 3 °C/h. Then the furnace was switched off and allowed to cool to room temperature. Single crystals of $Nd_2(MoO_4)(Te_4O_{10})$ (prismatic in shape and light purple in color) were initially prepared by the solid-state reaction of a mixture containing Nd_2O_3 (0.06 g, 0.18 mmol), MoO_3 (0.051 g, 0.35 mmol), and TeO_2 (0.223 g, 1.4 mmol) in an evacuated quartz tube at 720 °C for 6 days and then cooled to 300 °C at a cooling rate of 3.5 °C/h before the furnace was switched off. Results of EDS microprobe elemental analyses on single crystals of $Ln_2(MoO_4)(Te_4O_{10})$ (Ln = Pr, Nd) gave molar ratios of Ln/Mo/Te of 2.0:1.0:4.3 and 2.1:1.0:4.2 respectively for $Pr_2(MoO_4)(Te_4O_{10})$ and $Nd_2(MoO_4)(Te_4O_{10})$. After proper structural analyses, single-phase powder samples of $Ln_2(MoO_4)(Te_4O_{10})$ (Ln = Pr, Nd) were prepared quantitatively by reacting a mixture of Ln_2O_3/MoO_3/TeO_2 in a molar ratio of 1:1:4 at 720 and 600 °C for 6 days (Supporting Information). IR data (KBr, cm^{-1}) for $Pr_2(MoO_4)(Te_4O_{10})$ and $Nd_2(MoO_4)(Te_4O_{10})$ are listed in Table 1.

Table 1. IR Data (cm^{-1}) for the Eight Compounds

compound	IR (cm^{-1})
$Pr_2(MoO_4)(Te_4O_{10})$	911 (m), 852 (s), 803 (s), 768 (s), 735 (m), 708 (s), 663 (s), 634 (s), 596 (s), 467 (w)
$Nd_2(MoO_4)(Te_4O_{10})$	912 (m), 855 (vs), 803 (s), 771 (s), 737 (s), 709 (s), 663 (vs), 635 (vs), 597 (s), 471 (m), 445 (w), 432 (w), 410 (w)
$La_2(WO_4)(Te_3O_7)_2$	911 (w), 806 (vs), 764 (s), 665 (s), 626 (m), 508 (w)
$Nd_2W_2Te_2O_{13}$	933 (s), 909 (s), 848 (vs), 820 (vs), 771 (vs), 750 (vs), 722 (s), 677 (s), 647 (vs), 595 (vs), 504 (s), 476 (m), 459 (m), 436 (w), 417 (w)
$Pr_5(MoO_4)(Te_5O_{13})(TeO_3)_2Cl_3$	909 (m), 880 (s), 848 (s), 779 (s), 728 (vs), 685 (s), 635 (s), 598 (s), 488 (m), 440 (w), 422 (w), 407 (w)
$Pr_5(WO_4)(Te_5O_{13})(TeO_3)_2Cl_3$	937 (w), 880 (m), 845 (m), 779 (s), 750 (s), 728 (vs), 680 (s), 635 (s), 597 (s), 484 (w), 475 (w), 438 (w), 418 (w)
$Nd_5(MoO_4)(Te_5O_{13})(TeO_3)_2Cl_3$	910 (m), 880 (m), 847 (m), 780 (s), 752 (s), 729 (vs), 683 (s), 666 (s), 636 (s), 592 (s), 487 (m), 474 (m), 442 (w), 423 (w), 407 (w)
$Nd_5(WO_4)(Te_5O_{13})(TeO_3)_2Cl_3$	937 (w), 880 (m), 845 (m), 781(s), 752 (s), 729 (vs), 680 (s), 669 (s), 634 (s), 595 (s), 490 (w), 474 (w), 442 (w), 422 (w)

(9) (a) Wickleder, M. S.; Hamida, M. B. *Z. Anorg. Allg. Chem.* **2003**, *629*, 556. (b) Harrison, W. T. A.; Zhang, Z. H. *J. Solid State Chem.* **1997**, *133*, 572. (c) Berrigan, R.; Gatehouse, B. M. *Acta Crystallogr.* **1996**, *C52*, 496. (d) Ok, K. M.; Zhang, L.; Halasyamani, P. S. *J. Solid State Chem.* **2003**, *175*, 264.

(10) (a) Slooff, L. H.; Polman, A.; Oude Wolbers, M. P.; van Veggel, F. C. J. M.; Reinhoudt, D. N.; Hofstraat, J. W. *J. Appl. Phys.* **1997**, *83*, 497. (b) Slooff, L. H.; Polman, A.; Klink, S. I.; Hebink, G. A.; Grave, L.; van Veggel, F. C. J. M.; Reinhoudt, D. N.; Hofstraat, J. W. *Opt. Mater.* **2000**, *14*, 101.

(11) Shen, Y. L.; Jiang, H. L.; Xu, J.; Mao, J. G.; Cheah, K. W. *Inorg. Chem.* **2005**, *44*, 9314.

(12) (a) Zachariasen, W. H. *Acta Crystallogr.* **1949**, *2*, 388. (b) Meyer, G.; Schleid, T. *Z. Anorg. Allg. Chem.* **1986**, *533*, 181.

Table 2. Crystal Data and Structure Refinements for the Eight Compounds

formula	$Pr_2MoTe_4O_{14}$	$Nd_2MoTe_4O_{14}$	$La_2WTe_6O_{18}$	$Nd_2W_2Te_2O_{13}$	$Pr_5MoTe_7O_{23}Cl_3$	$Pr_5WTe_7O_{23}Cl_3$	$Nd_5MoTe_7O_{23}Cl_3$	$Nd_5WTe_7O_{23}Cl_3$
fw	1112.16	1118.82	1515.27	1119.38	2168.04	2255.95	2184.69	2272.60
cryst syst	triclinic	triclinic	hexagonal	triclinic	monoclinic	monoclinic	monoclinic	monoclinic
space group	$P\bar{1}$	$P\bar{1}$	$P\bar{3}c1$	$P\bar{1}$	$C2/m$	$C2/m$	$C2/m$	$C2/m$
a (Å)	6.9894(18)	6.9494(18)	6.8415(4)	6.647(3)	7.6400(15)	7.669(2)	7.6400(8)	7.635(3)
b (Å)	9.964(3)	9.931(3)	6.8415(4)	6.905(3)	18.200(4)	18.261(6)	18.1961(16)	18.211(6)
c (Å)	10.157(3)	10.116(3)	19.958(2)	11.525(5)	18.210(4)	18.324(6)	18.2082(19)	18.217(9)
α (deg)	89.669(7)	89.719(7)	90	90.307(7)	90	90	90	90
β (deg)	72.434(6)	72.531(6)	90	98.116(6)	97.04(3)	97.0370(10)	97.042(6)	96.866(6)
γ (deg)	86.546(7)	86.593(7)	120	93.658(10)	90	90	90	90
V (Å^3)	673.1(3)	664.7(3)	809.0(1)	522.5(4)	2513.0(9)	2547(1)	2512.2(4)	2515(2)
Z	2	2	2	2	4	4	4	4
D_c (g·cm^{-3})	5.488	5.590	6.220	7.115	5.730	5.883	5.776	6.003
μ(Mo Kα) (mm^{-1})	16.609	17.299	22.977	37.261	18.369	22.144	19.012	23.065
GOF on F^2	1.015	1.025	1.099	1.036	1.051	1.105	1.080	0.959
R1, wR2 [$I > 2\sigma(I)$][a]	0.0210, 0.0441	0.0199, 0.0405	0.0255, 0.0573	0.0197, 0.0438	0.0249, 0.0584	0.0270, 0.0524	0.0378, 0.0706	0.0225, 0.0446
R1, wR2 (all data)	0.0248, 0.0454	0.0249, 0.0420	0.0290, 0.0591	0.0244, 0.0449	0.0289, 0.0604	0.0375, 0.0562	0.0504, 0.0759	0.0278, 0.0455

[a] $R1 = \sum||F_o| - |F_c||/\sum|F_o|$, $wR2 = \{\sum w[(F_o)^2 - (F_c)^2]^2/\sum w[(F_o)^2]^2\}^{1/2}$.

Preparation of $La_2(WO_4)(Te_3O_7)_2$. Colorless plate-shaped single crystals of $La_2(WO_4)(Te_3O_7)_2$ were initially prepared together with some other unidentified powders by the solid-state reaction of a mixture containing La_2O_3 (0.098 g, 0.3 mmol), WO_3 (0.139 g, 0.6 mmol), and TeO_2 (0.239 g, 1.5 mmol) in an evacuated quartz tube at 750 °C for 6 days and then cooled to 350 °C at 4 °C/h before the furnace was switched off. The atomic ratio of La/W/Te determined by EDS is 2.0:1.3:5.8, which is in good agreement with the one determined from single-crystal X-ray structural analysis. After proper structural analysis, a pure-powder sample of $La_2(WO_4)(Te_3O_7)_2$ was obtained quantitatively by the solid-state reaction of a mixture of $La_2O_3/WO_3/TeO_2$ in a molar ratio of 1:1:6 at 650 °C for 6 days. Its purity was confirmed by powder XRD studies (Supporting Information). IR data (KBr, cm^{-1}) for $La_2(WO_4)(Te_3O_7)_2$ are listed in Table 1.

Preparation of $Nd_2W_2Te_2O_{13}$. Single crystals of $Nd_2W_2Te_2O_{13}$ (prismatic in shape and light purple in color) were initially obtained together with some other unidentified powders by the solid-state reaction of a mixture composed of Nd_2O_3 (0.084 g, 0.25 mmol), WO_3 (0.116 g, 0.5 mmol), and TeO_2 (0.200 g, 1.25 mmol) in an evacuated quartz tube at 720 °C for 6 days. It was allowed to cool down to 300 °C at 3.5 °C/h before the furnace was switched off. EDS microprobe analyses gave a molar ratio of Nd/W/Te of 1.0: 0.9: 1.3. After proper structural analyses, a pure-powder sample of $Nd_2W_2Te_2O_{13}$ was prepared by the solid-state reaction of a mixture of $Nd_2O_3/WO_3/TeO_2$ in a molar ratio of 1:2:2 at 720 °C for 6 days (Supporting Information). IR data (KBr, cm^{-1}) for $Nd_2W_2Te_2O_{13}$ are reported in Table 1.

Preparation of $Ln_5(MO_4)(Te_5O_{13})(TeO_3)_2Cl_3$ (Ln = Pr, Nd; M = Mo, W). Single crystals of $Pr_5(MoO_4)(Te_5O_{13})(TeO_3)_2Cl_3$ (needlelike in shape and light green in color) and $Pr_5(WO_4)(Te_5O_{13})(TeO_3)_2Cl_3$ (bricklike in shape and light green in color) were initially obtained together with some other unidentified powders obtained by the solid-state reaction of a mixture containing PrOCl (0.096 g, 0.5 mmol), MoO_3 or WO_3 (0.4 mmol), and TeO_2 (0.191 g, 1.2 mmol) in an evacuated quartz tube at 750 or 720 °C for 6 days and then slowly cooled to room temperature at a cooling rate of 4.0 or 4.5 °C/h, respectively. Single crystals of $Nd_5(MoO_4)(Te_5O_{13})(TeO_3)_2Cl_3$ (needlelike in shape and light purple in color) and $Nd_5(WO_4)(Te_5O_{13})(TeO_3)_2Cl_3$ (bricklike in shape and light purple in color) were prepared together with some other unidentified powders by the solid-state reaction of a mixture containing of NdOCl (0.100 g, 0.5 mmol), MoO_3 (0.043 g, 0.3 mmol) or WO_3 (0.070 g, 0.3 mmol), and TeO_2 (0.192 g, 1.2 mmol) in an evacuated quartz tube at 750 °C or 720 °C for 6 days and then both cooled to 310 °C at a cooling rate of 3.5 °C/h before the furnace was switched off. EDS microprobe analyses gave molar ratios of Ln/M/Te/Cl of 5.2:1.0:7.3:3.2, 4.9:1.0:7.3:3.1, 5.3:1.0:7.4:3.1, and 4.8:1.0:7.3:2.9 respectively for $Pr_5(MoO_4)(Te_5O_{13})(TeO_3)_2Cl_3$, $Pr_5(WO_4)(Te_5O_{13})(TeO_3)_2Cl_3$, $Nd_5(MoO_4)(Te_5O_{13})(TeO_3)_2Cl_3$, and $Nd_5(WO_4)(Te_5O_{13})(TeO_3)_2Cl_3$. After proper structural analyses, pure powder samples of the above compounds were prepared quantitatively by reacting a mixture of $Ln_2O_3/LnOCl/MO_3/TeO_2$ in a molar ratio of 1:3:1:7 at 710−730 °C for 6 days (Supporting Information). IR data for the above four compounds are listed in Table 1.

Single-Crystal Structure Determination. Data collections for the eight compounds were performed on either a Rigaku Mercury CCD diffractometer or a Rigaku Saturn70 CCD (for $Nd_2W_2Te_2O_{13}$ and $Nd_5(WO_4)(Te_5O_{13})(TeO_3)_2Cl_3$) or a Siemens Smart CCD (for $Pr_5(MoO_4)(Te_5O_{13})(TeO_3)_2Cl_3$) equipped with graphite-monochromated Mo Kα radiation ($\lambda = 0.71073$ Å) at 293 K. These data sets were corrected for Lorentz and polarization factors as well as for absorption by the multiscan method or ψ-scan technique for $Pr_5(MoO_4)(Te_5O_{13})(TeO_3)_2Cl_3$ or numerical absorption for $Nd_5(WO_4)(Te_5O_{13})(TeO_3)_2Cl_3$.[13a] All of the structures were solved by direct methods and refined by full-matrix least-squares fitting on F^2 by *SHELX-97*.[13b] All of the atoms were refined with anisotropic thermal parameters. In $La_2(WO_4)(Te_3O_7)_2$, W(1) is disordered and displays two orientations at (0, 0, 0.275601) and (0, 0, 0.22440); both are close to the (0, 0, 0.25) site with an interatomic distance of 1.0219(16) Å. Hence, its occupancy factor is reduced by 50%. Likewise, Cl(4) in $Ln_5(MO_4)(Te_5O_{13})(TeO_3)_2Cl_3$ (Ln = Pr, Nd; M = Mo, W) is also disordered and displays two orientations close to the ($^1/_4$, $^1/_4$, $^1/_4$) site with the interatomic Cl···Cl distances in the range of 1.08(2)−1.43(2) Å. Hence, its occupancy factor is also reduced by 50%. Crystallographic data and structural refinements for all of the compounds are summarized in Table 2. Important bond distances are listed in Table 3. More details on the crystallographic studies as well as atomic displacement parameters are given as Supporting Information.

Results and Discussion

Solid-state reactions of lanthanide(III) oxide (and/or lanthanide(III) oxychloride), MoO_3 (or WO_3), and TeO_2 at high temperature led to eight new compounds with four different types of structures, namely, $Ln_2(MoO_4)(Te_4O_{10})$ (Ln = Pr,

(13) (a) *CrystalClear*, version 1.3.5.; Rigaku Corp.: Woodlands, TX, 1999. (b) Sheldrick, G. M. *SHELXTL, Crystallographic Software Package*, version 5.1; Bruker-AXS: Madison, WI, 1998.

Nd), $La_2(WO_4)(Te_3O_7)_2$, $Nd_2W_2Te_2O_{13}$, and $Ln_5(MO_4)(Te_5O_{13})(TeO_3)_2Cl_3$ (Ln = Pr, Nd; M = Mo, W). The first two compounds differ from $Ln_2MoTe_3O_{12}$ reported previously by our group in that they contain one additional TeO_2 in their chemical compositions.[11] Such a slight change resulted in a totally different structure. $La_2(WO_4)(Te_3O_7)_2$ and $Nd_2W_2Te_2O_{13}$ represent the first examples of lanthanide(III) tellurium(IV) oxides decorated by WO_4 tetrahedra or

Table 3. Important Bond Lengths (Angstroms) for the Eight Compounds[a]

$Pr_2(MoO_4)(Te_4O_{10})$

Pr(1)−O(2)#1	2.406(4)	Pr(1)−O(12)#2	2.406(4)
Pr(1)−O(10)	2.442(4)	Pr(1)−O(4)	2.450(4)
Pr(1)−O(5)#3	2.462(3)	Pr(1)−O(11)#1	2.471(4)
Pr(1)−O(1)#3	2.577(3)	Pr(1)−O(6)	2.611(3)
Pr(2)−O(8)#1	2.262(4)	Pr(2)−O(4)#5	2.377(3)
Pr(2)−O(2)#1	2.443(4)	Pr(2)−O(9)	2.499(3)
Pr(2)−O(1)	2.503(3)	Pr(2)−O(6)	2.577(3)
Pr(2)−O(5)	2.591(3)	Pr(2)−O(10)#5	2.822(4)
Mo(1)−O(13)	1.738(4)	Mo(1)−O(11)#6	1.775(4)
Mo(1)−O(14)	1.741(4)	Mo(1)−O(12)	1.758(4)
Te(1)−O(1)#4	1.857(3)	Te(1)−O(2)#2	1.855(4)
Te(1)−O(3)	1.917(3)	Te(2)−O(3)	1.989(4)
Te(2)−O(4)	1.862(3)	Te(2)−O(6)	2.462(4)
Te(2)−O(5)	1.878(4)	Te(3)−O(6)	1.887(3)
Te(3)−O(8)	1.830(4)	Te(3)−O(9)	2.375(3)
Te(3)−O(7)	2.032(4)	Te(4)−O(7)#5	1.944(3)
Te(4)−O(9)	1.864(4)	Te(4)−O(10)#5	1.871(3)

$Nd_2(MoO_4)(Te_4O_{10})$

Nd(1)−O(2)#1	2.378(3)	Nd(1)−O(12)#2	2.385(4)
Nd(1)−O(10)	2.421(4)	Nd(1)−O(4)	2.434(3)
Nd(1)−O(5)#3	2.434(3)	Nd(1)−O(11)#1	2.458(4)
Nd(1)−O(1)#3	2.560(3)	Nd(1)−O(6)	2.596(3)
Nd(2)−O(8)#1	2.251(3)	Nd(2)−O(4)#5	2.352(3)
Nd(2)−O(2)#1	2.422(3)	Nd(2)−O(1)	2.473(3)
Nd(2)−O(9)	2.487(4)	Nd(2)−O(6)	2.559(3)
Nd(2)−O(5)	2.575(3)	Nd(2)−O(10)#5	2.813(4)
Mo(1)−O(13)	1.733(4)	Mo(1)−O(14)	1.746(4)
Mo(1)−O(12)	1.757(4)	Mo(1)−O(11)#6	1.779(4)
Te(1)−O(1)#4	1.856(3)	Te(1)−O(2)#2	1.859(3)
Te(1)−O(3)	1.926(3)	Te(2)−O(3)	1.972(3)
Te(2)−O(4)	1.867(3)	Te(2)−O(5)	1.887(3)
Te(2)−O(6)	2.457(3)	Te(3)−O(6)	1.879(3)
Te(3)−O(8)	1.826(3)	Te(3)−O(7)	2.035(3)
Te(3)−O(9)	2.345(3)	Te(4)−O(7)#5	1.937(3)
Te(4)−O(9)	1.864(3)	Te(4)−O(10)#5	1.872(3)

$Nd_2W_2Te_2O_{13}$

Nd(1)−O(4)	2.333(5)	Nd(1)−O(2)#1	2.422(5)
Nd(1)−O(11)#2	2.448(5)	Nd(1)−O(8)#3	2.450(5)
Nd(1)−O(13)#2	2.479(5)	Nd(1)−O(1)	2.526(5)
Nd(1)−O(3)	2.562(5)	Nd(1)−O(8)#4	2.580(5)
Nd(2)−O(5)#5	2.407(5)	Nd(2)−O(3)	2.423(5)
Nd(2)−O(10)	2.438(6)	Nd(2)−O(12)	2.456(5)
Nd(2)−O(6)#6	2.485(5)	Nd(2)−O(4)	2.523(5)
Nd(2)−O(5)	2.545(5)	Nd(2)−O(7)#5	2.615(5)
Nd(2)−O(9)	2.681(5)		
W(1)−O(10)	1.743(6)	W(1)−O(7)	1.776(5)
W(1)−O(13)	1.834(5)	W(1)−O(6)	2.033(5)
W(1)−O(12)#4	2.081(5)	W(1)−O(1)	2.300(5)
W(2)−O(11)	1.747(5)	W(2)−O(9)#7	1.767(5)
W(2)−O(8)#7	1.900(5)	W(2)−O(12)	1.930(5)
W(2)−O(2)	2.172(5)	W(2)−O(13)#6	2.232(5)
Te(1)−O(3)	1.863(5)	Te(1)−O(1)#6	1.898(5)
Te(1)−O(2)	1.936(5)	Te(1)−O(8)	2.516(5)
Te(2)−O(5)	1.846(5)	Te(2)−O(4)	1.863(5)
Te(2)−O(6)	1.921(5)		

$Pr_5(MoO_4)(Te_5O_{13})(TeO_3)_2Cl_3$

Pr(1)−O(1)	2.353(6)	Pr(1)−O(1)#1	2.353(6)
Pr(1)−O(4)#1	2.364(6)	Pr(1)−O(4)	2.364(6)
Pr(1)−O(1)#2	2.439(6)	Pr(1)−O(1)#3	2.439(6)
Pr(1)−O(3)#4	2.681(6)	Pr(1)−O(3)#5	2.681(6)
Pr(2)−O(8)#6	2.350(6)	Pr(2)−O(7)	2.413(5)
Pr(2)−O(10)#2	2.440(6)	Pr(2)−O(12)#7	2.440(6)
Pr(2)−O(5)	2.475(6)	Pr(2)−O(13)#6	2.488(5)
Pr(2)−O(9)	2.563(6)	Pr(2)−Cl(2)	3.009(2)
Pr(3)−O(2)	2.378(6)	Pr(3)−O(2)#2	2.392(6)
Pr(3)−O(9)	2.536(6)	Pr(3)−O(4)	2.576(6)
Pr(3)−O(5)#5	2.603(6)	Pr(3)−O(10)	2.603(6)
Pr(3)−O(5)	2.635(6)	Pr(3)−O(10)#2	2.660(6)
Pr(3)−O(3)#5	2.917(6)	Pr(3)−O(8)#2	2.942(8)
Mo(1)−O(11)	1.715(9)	Mo(1)−O(12)#9	1.744(6)
Mo(1)−O(12)#10	1.744(6)	Mo(1)−O(13)	1.829(8)
Te(1)−O(1)	1.852(6)	Te(1)−O(2)	1.874(6)
Te(1)−O(3)#11	1.931(6)	Te(2)−O(4)	1.859(6)
Te(2)−O(5)	1.876(6)	Te(2)−O(6)	2.093(6)
Te(2)−O(3)	2.142(6)	Te(3)−O(7)	1.867(9)
Te(3)−O(6)#8	1.898(6)	Te(3)−O(6)	1.898(6)
Te(4)−O(8)	1.851(7)	Te(4)−O(9)	1.874(6)
Te(4)−O(10)	1.878(6)		

$Pr_5(WO_4)(Te_5O_{13})(TeO_3)_2Cl_3$

Pr(1)−O(1)	2.356(5)	Pr(1)−O(1)#1	2.356(5)
Pr(1)−O(4)#1	2.382(4)	Pr(1)−O(4)	2.382(4)
Pr(1)−O(1)#2	2.434(5)	Pr(1)−O(1)#3	2.434(5)
Pr(1)−O(3)#4	2.706(5)	Pr(1)−O(3)#5	2.706(5)
Pr(2)−O(8)#6	2.367(6)	Pr(2)−O(12)#7	2.423(5)
Pr(2)−O(7)	2.426(3)	Pr(2)−O(10)#2	2.437(5)
Pr(2)−O(5)	2.482(4)	Pr(2)−O(13)#6	2.506(4)
Pr(2)−O(9)	2.564(5)	Pr(2)−Cl(2)	3.030(2)
Pr(3)−O(2)	2.391(5)	Pr(3)−O(2)#2	2.397(5)
Pr(3)−O(9)	2.543(5)	Pr(3)−O(4)	2.592(5)
Pr(3)−O(10)	2.620(5)	Pr(3)−O(5)#4	2.623(5)
Pr(3)−O(5)	2.643(5)	Pr(3)−O(10)#2	2.680(5)
Pr(3)−O(3)#4	2.935(5)	Pr(3)−O(8)#2	2.971(6)
W(1)−O(11)	1.733(9)	W(1)−O(12)#9	1.775(5)
W(1)−O(12)#10	1.775(5)	W(1)−O(13)	1.849(6)
Te(1)−O(1)	1.865(5)	Te(1)−O(2)	1.881(4)
Te(1)−O(3)#11	1.942(5)	Te(2)−O(4)	1.853(5)
Te(2)−O(5)	1.888(4)	Te(2)−O(6)	2.111(5)
Te(2)−O(3)	2.138(5)	Te(3)−O(7)	1.870(6)
Te(3)−O(6)#8	1.899(5)	Te(3)−O(6)	1.899(5)
Te(4)−O(8)	1.861(5)	Te(4)−O(9)	1.880(5)
Te(4)−O(10)	1.889(5)		

$Nd_5(MoO_4)(Te_5O_{13})(TeO_3)_2Cl_3$

Nd(1)−O(1)	2.344(6)	Nd(1)−O(1)#1	2.344(6)
Nd(1)−O(4)#1	2.369(6)	Nd(1)−O(4)	2.369(6)
Nd(1)−O(1)#2	2.423(7)	Nd(1)−O(1)#3	2.423(7)
Nd(1)−O(3)#4	2.639(6)	Nd(1)−O(3)#5	2.639(6)
Nd(2)−O(8)#6	2.364(7)	Nd(2)−O(7)	2.406(5)
Nd(2)−O(10)#2	2.412(7)	Nd(2)−O(12)#7	2.432(6)
Nd(2)−O(5)	2.464(6)	Nd(2)−O(13)#6	2.488(5)
Nd(2)−O(9)	2.549(7)	Nd(2)−Cl(2)	3.015(2)
Nd(3)−O(2)	2.369(6)	Nd(3)−O(2)#2	2.387(6)
Nd(3)−O(9)	2.537(7)	Nd(3)−O(4)	2.574(6)
Nd(3)−O(5)#4	2.607(6)	Nd(3)−O(10)	2.608(7)
Nd(3)−O(5)	2.624(6)	Nd(3)−O(10)#2	2.662(7)
Nd(3)−O(3)#4	2.912(7)	Nd(3)−O(8)#2	2.937(8)
Mo(1)−O(11)	1.714(10)	Mo(1)−O(12)#9	1.751(7)
Mo(1)−O(12)#10	1.751(7)	Mo(1)−O(13)	1.845(9)
Te(1)−O(1)	1.866(6)	Te(1)−O(2)	1.887(6)
Te(1)−O(3)#11	1.940(7)	Te(2)−O(4)	1.857(6)
Te(2)−O(5)	1.889(6)	Te(2)−O(6)	2.100(7)
Te(2)−O(3)	2.162(6)	Te(3)−O(7)	1.869(9)
Te(3)−O(6)#8	1.899(7)	Te(3)−O(6)	1.899(7)
Te(4)−O(8)	1.845(8)	Te(4)−O(9)	1.886(6)
Te(4)−O(10)	1.900(6)		

Table 3 (Continued)

$Nd_5(WO_4)(Te_5O_{13})(TeO_3)_2Cl_3$				$La_2(WO_4)(Te_3O_7)_2$			
Nd(1)−O(1)	2.343(4)	Nd(1)−O(1)#1	2.343(4)	La(1)−O(3)#5	2.487(4)	La(1)−O(3)	2.487(4)
Nd(1)−O(4)#1	2.364(4)	Nd(1)−O(4)	2.364(4)	La(1)−O(3)#2	2.487(4)	La(1)−O(3)#6	2.615(4)
Nd(1)−O(1)#2	2.425(4)	Nd(1)−O(1)#3	2.425(4)	La(1)−O(3)#7	2.615(4)	La(1)−O(3)#8	2.615(4)
Nd(1)−O(3)#4	2.649(4)	Nd(1)−O(3)#5	2.649(4)	La(1)−O(4)	2.659(4)	La(1)−O(4)#5	2.659(4)
Nd(2)−O(8)#6	2.343(5)	Nd(2)−O(12)#7	2.400(4)	La(1)−O(4)#2	2.659(4)	La(1)−O(1)#1	2.884(8)
Nd(2)−O(7)	2.412(3)	Nd(2)−O(10)#2	2.420(4)	W(1)−O(4)#2	1.724(6)	W(1)−O(4)#3	1.724(6)
Nd(2)−O(5)	2.460(4)	Nd(2)−O(13)#6	2.504(4)	W(1)−O(4)#4	1.724(6)	W(1)−O(5)	1.786(12)
Nd(2)−O(9)	2.531(4)	Nd(2)−Cl(2)	3.0190(17)	Te(1)−O(3)	1.850(4)	Te(1)−O(2)	1.891(4)
Nd(3)−O(2)	2.378(4)	Nd(3)−O(2)#2	2.388(4)	Te(1)−O(2)#2	2.140(4)	Te(1)−O(1)#9	2.193(1)
Nd(3)−O(9)	2.529(4)	Nd(3)−O(4)	2.583(4)				
Nd(3)−O(10)	2.601(5)	Nd(3)−O(5)#4	2.605(4)				
Nd(3)−O(5)	2.633(4)	Nd(3)−O(10)#2	2.663(5)				
Nd(3)−O(3)#4	2.935(4)	Nd(3)−O(8)#2	2.963(6)				
W(1)−O(11)	1.726(7)	W(1)−O(12)#9	1.779(4)				
W(1)−O(12)#10	1.779(4)	W(1)−O(13)	1.844(6)				
Te(1)−O(1)	1.868(4)	Te(1)−O(2)	1.876(4)				
Te(1)−O(3)#11	1.947(4)	Te(2)−O(4)	1.859(4)				
Te(2)−O(5)	1.894(4)	Te(2)−O(6)	2.107(4)				
Te(2)−O(3)	2.143(4)	Te(3)−O(7)	1.869(6)				
Te(3)−O(6)#8	1.892(4)	Te(3)−O(6)	1.892(4)				
Te(4)−O(8)	1.861(5)	Te(4)−O(9)	1.895(4)				
Te(4)−O(10)	1.896(4)						

[a] Symmetry operators used to generate equivalent atoms: For $Ln_2(MoO_4)(Te_4O_{10})$(Ln = Pr, Nd): #1 $-x+1, -y+1, -z+1$; #2 $x, y, z-1$; #3 $-x+1, -y+1, -z$; #4 $x-1, y, z$; #5 $x+1, y, z$; #6 $x, y-1, z$. For $La_2(WO_4)(Te_3O_7)_2$: #1 $y, x, -z+1/2$; #2 $-y+1, x-y+1, z$; #3 $-x+y-1, -x, z$; #4 $x, y-1, z$; #5 $-x+y, -x+1, z$; #6 $y, x+1, -z+1/2$; #7 $-x, -x+y, -z+1/2$; #8 $x-y+1, -y+1, -z+1/2$; #9 $x-1, y, z$. For $Nd_2W_2Te_2O_{13}$: #1 $-x+1, -y+1, -z$; #2 $x, y-1, z$; #3 $-x+1, -y, -z$; #4 $x-1, y, z$; #5 $-x+1, -y+1, -z+1$; #6 $x+1, y, z$; #7 $x, y+1, z$. For $Ln_5(MO_4)(Te_5O_{13})(TeO_3)_2Cl_3$ (Ln = Pr, Nd; M = Mo, W): #1 $-x+1, y, -z+1$; #2 $x-1/2, -y+1/2, z$; #3 $-x+3/2, -y+1/2, -z+1$; #4 $-x+1/2, -y+1/2, -z+1$; #5 $x+1/2, -y+1/2, z$; #6 $x-1, y, z$; #7 $-x+1, -y+1, -z+1$; #8 $x, -y+1, z$; #9 $x, -y+1, z-1$; #10 $x, y, z-1$; #11 $x+1, y, z$.

WO_6 octahedra. $Ln_5(MO_4)(Te_5O_{13})(TeO_3)_2Cl_3$ (Ln = Pr, Nd; M = Mo, W) are the first examples of structurally characterized lanthanide(III) molybdenum (or tungsten) tellurium(IV) oxyhalides. On the basis of powder XRD diffraction studies, all eight compounds have been successfully obtained as single phases (Supporting Information).

The syntheses of isotypic $Ln_2(MoO_4)(Te_4O_{10})$ (Ln = Pr, Nd) can be expressed by the following reaction at 720 or 600 °C: $Ln_2O_3 + MoO_3 + 4TeO_2 \rightarrow Ln_2(MoO_4)(Te_4O_{10})$. Their structures are different from those of $Ln_2MoTe_3O_{12}$ (Ln = La, Nd) and feature a 3D network in which the Ln(III) ions are interconnected by 1D $Te_4O_{10}^{4-}$ chains and MoO_4 tetrahedra (Figure 1). The structure of $Nd_2(MoO_4)(Te_4O_{10})$ will be discussed in detail as a representative. There are two unique Nd(III) atoms in its asymmetric unit; Nd(1) is eight-coordinated by eight tellurite O atoms, whereas Nd(2) is eight-coordinated by six tellurite O atoms and two O atoms from two molybdate anions. The Nd−O distances range from 2.251(3) to 2.813(4) Å (Table 3), which are comparable to those in other neodymium(III) tellurites reported.[11,14] The Mo(VI) atom is in a slightly distorted tetrahedral coordination environment with Mo−O distances in the range of 1.733(4)−1.779(4) Å (Table 3), which are close to those reported previously.[11] Te(1) and Te(4) are coordinated by three O atoms in a distorted ψ-TeO_3 tetrahedral geometry, whereas Te(2) and Te(3) are coordinated by four O atoms in a distorted ψ-TeO_4 tetragonal-pyramidal geometry. The Te−O distances are in the range of 1.826(3)−2.457(3) Å. Bond valence calculations indicate that the Mo atom is in an oxidation state of 6+ and the Te atoms are 4+; the calculated total bond valences are 6.06, 3.91, 3.91, 4.03, and 3.80 respectively for Mo(1), Te(1), Te(2), Te(3), and Te(4).[15]

$Te(3)O_4$ and $Te(4)O_3$ groups are interconnected via corner-sharing (O(7) and O(9)), leading to a linear chain. $Te(1)O_3$ and $Te(2)O_4$ groups form a dimer by corner-sharing (O(3)). The dimers are hanging on the same side of the linear chain through corner-sharing O(6) atoms, resulting in the formation of a 1D $Te_4O_{10}^{4-}$ anionic chain (Figure 1a). To our knowledge, such a type of 1D tellurium(IV) oxide anionic chain has not been reported before. The interconnection of Nd(1) and Nd(2) atoms via bridging $Te_4O_{10}^{4-}$ anionic chains leads to a (020) neodymium(III) tellurium(IV) oxide layer. Such neighboring layers are further bridged by MoO_4 tetrahedra into a 3D network with apertures along the *a* axis. The aperture is formed by 10-membered rings containing four Nd(1), two Nd(2), two MoO_4^{2-} anions, and two Te(3)-O_4 groups. The lone pairs of the Te(IV) atoms are orientated toward the apertures of the structure (Figure 1b). The effective volume of a lone pair is approximately the same as the volume of an O^{2-} anion according to Galy et al.[16]

It is worth comparing the structures of $Ln_2(MoO_4)(Te_4O_{10})$ (Ln = Pr, Nd) with those of $La_2MoTe_3O_{12}$ and $Nd_2MoTe_3O_{12}$. All four compounds contain MoO_4 tetrahedra; however, their Te−O architectures are completely different: $La_2MoTe_3O_{12}$ features discrete $Te_3O_8^{4-}$ anions, whereas

(14) (a) Shen, Y. L.; Mao, J. G. *Inorg. Chem.* **2005**, *44*, 5328. (b) Castro, A.; Enjalbert, R.; Lloyd, D.; Rasines, I.; Galy, J. *J. Solid State Chem.* **1990**, *85*, 100. (c) Tarasov, I. V.; Dolgikh, V. A.; Aksel'rud, L. G.; Berdonosov, P. S.; Ponovkin, B. A. *Z. Neorg. Khim.* **1996**, *41*, 1243. (d) Berdonosov, P. S.; Charkin, D. O.; Kusainova, A. M.; Hervoches, C. H.; Dolgikh, V. A.; Lightfoot, P. *Solid State Sci.* **2000**, *2*, 553.

(15) (a) Brese, N. E.; O'Keeffe, M. *Acta Crystallogr.* **1991**, *B47*, 192. (b) Brown, I. D.; Altermatt, D. *Acta Crystallogr.* **1985**, *B41*, 244.

(16) Galy, J.; Meunier, G.; Andersson, S.; Åström, A. *J. Solid State Chem.* **1975**, *13*, 142.

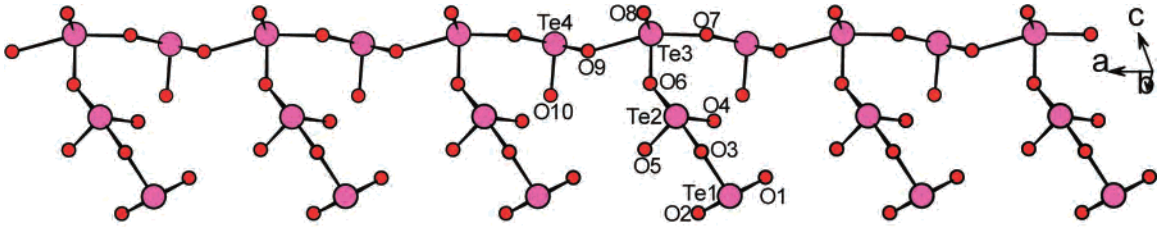

(a)

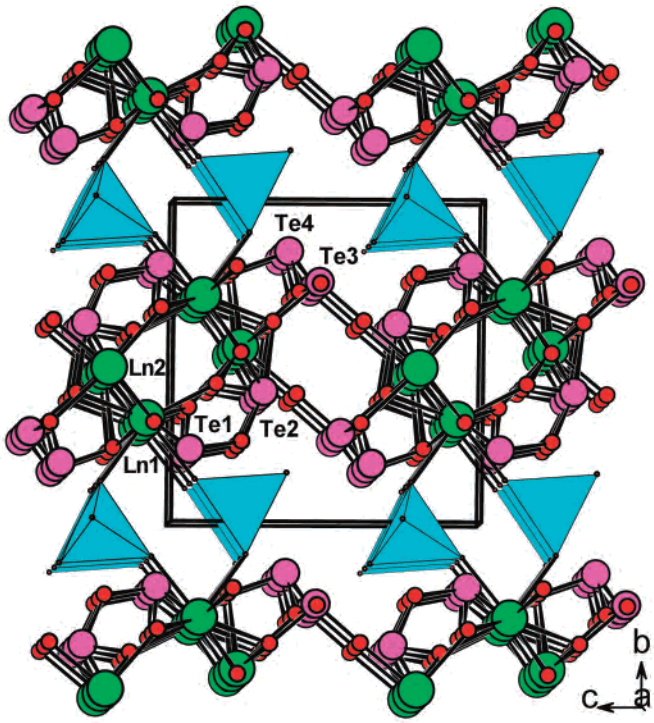

(b)

Figure 1. (a) 1D chain of the $Te_4O_{10}^{4-}$ anion in $Ln_2(MoO_4)(Te_4O_{10})$ (Ln = Pr, Nd); (b) view of the structure of $Ln_2(MoO_4)(Te_4O_{10})$ down the *a* axis. The MoO_4 tetrahedra are shaded in cyan. Ln, Te, and O atoms are drawn as green, pink, and red circles, respectively.

$Nd_2MoTe_3O_{12}$ contains both TeO_3^{2-} anions and dimeric $Te_2O_5^{2-}$ anions,[11] and 1D $Te_4O_{10}^{4-}$ anions are found in $Ln_2(MoO_4)(Te_4O_{10})$ (Ln = Pr, Nd). $Nd_2MoTe_3O_{12}$ features a layered structure with MoO_4 tetrahedra hanging between two neighboring layers, whereas the MoO_4 tetrahedra in $La_2MoTe_3O_{12}$ are located at the tunnels of lanthanum(III) tellurium(IV) oxide.[11] In $Ln_2(MoO_4)(Te_4O_{10})$ (Ln = Pr, Nd), the MoO_4 tetrahedron serves as a bridge between two lanthanide(III) tellurium(IV) oxide layers.

$La_2(WO_4)(Te_3O_7)_2$ was obtained during our attempts to prepare the W(VI) analogue of $La_2MoTe_3O_{12}$. The synthesis of $La_2(WO_4)(Te_3O_7)_2$ can be expressed by the following reaction at 650 °C: $La_2O_3 + WO_3 + 6TeO_2 \rightarrow La_2(WO_4)(Te_3O_7)_2$. The La(1) atom lying in a position with a 3-fold symmetry is 10-coordinated by seven O atoms from two $Te_3O_7^{2-}$ anions and three O atoms from three WO_4 tetrahedra. The La−O distances are in the range from 2.487(4) to 2.884(8) Å (Table 3). The disordered W(1) atom is tetrahedrally coordinated by four O atoms with W−O distances ranging from 1.724(6) to 1.786(1) Å (Table 3), which are comparable to those in other tungsten tellurites.[4a,b,6c] The Te(1) atom is coordinated by four O atoms in a distorted ψ-TeO_4 tetragonal-pyramidal geometry, with the lone pair of Te(IV) occupying the pyramidal site. The Te−O distances are in the range of 1.850(4)−2.193(1) Å. The oxidation states of W and Te atoms are 6+ and 4+, respectively, according to bond valence calculations.[15] The calculated total bond valences for W(1) and Te(1) are 6.55 and 3.87, respectively.

The TeO_4 polyhedra are interconnected into a $Te_3O_7^{2-}$ layer via corner-sharing (Figure 2a). Three TeO_4 groups are interconnected via corner-sharing (O(2)) into a three-membered ring. These three-membered rings are further interconnected via corner-sharing (O(1)) into a 2D $Te_3O_7^{2-}$ anionic layer, resulting in the formation of a pear-shaped six-membered ring (Figure 2a). Similar Te_3 and pear-shaped Te_6 rings have been reported in $Cd_7Cl_8(Te_7O_{17})$.[17]

The interconnection of La^{3+} ions by bridging WO_4^{2-} anions led to a 2D $[La_2WO_4]^{4+}$ layer along the *ab* plane

(17) Jiang, H. L.; Mao, J. G. *Inorg. Chem.* **2006**, *45*, 717.

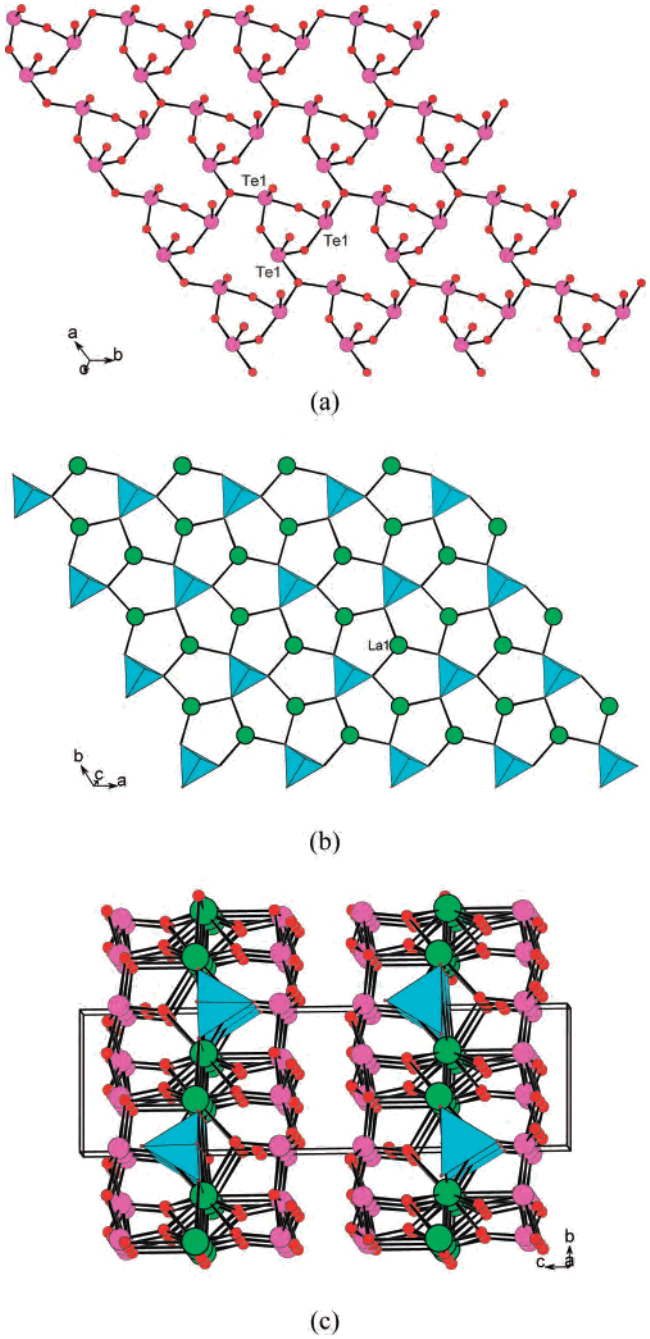

Figure 2. (a) 2D layer of the $Te_3O_7^{2-}$ anion; (b) $[La_2WO_4]^{4+}$ anion layer; (c) view of the structure of $La_2(WO_4)(Te_3O_7)_2$ down the *a* axis. The WO_4 tetrahedra are shaded in cyan. La, Te, and O atoms are drawn as green, pink, and red circles, respectively.

(Figure 2b). One $[La_2WO_4]^{4+}$ layer and two $Te_3O_7^{2-}$ layers are further interconnected into a thick triple layer in the *ab* plane via La−O−Te bridges (Figure 2c). The thickness of the layer is about 7.65 Å, and the interlayer opening width is about 3.0 Å. Such types of triple layers can also be viewed as the $[La_2WO_4]^{4+}$ layer being sandwiched between two $Te_3O_7^{2-}$ anionic layers. The lone-pair electrons of Te(IV) atoms are oriented toward the interlayer space (Figure 2c).

$Nd_2W_2Te_2O_{13}$ with a different structure was obtained in our attempts to prepare the Nd(III) analogue of $La_2(WO_4)(Te_3O_7)_2$. The synthesis of $Nd_2W_2Te_2O_{13}$ can be expressed by the following reaction at 720 °C: $Nd_2O_3 + 2WO_3 + 2TeO_2 \rightarrow Nd_2W_2Te_2O_{13}$. $Nd_2W_2Te_2O_{13}$ features a 3D network structure in which the W_2O_{10} dimers occupy the large apertures formed by neodymium tellurite (Figure 3b). There are two unique Nd^{3+} ions in its asymmetric unit; Nd(1) is eight-coordinated by four tellurite O atoms and four terminal O^{2-} of the WO_4^{2-} anions, whereas Nd(2) is nine-coordinated by five O atoms from four tellurite groups and four terminal O^{2-} of the WO_4^{2-} anions. The Nd−O distances range from 2.333(5) to 2.681(5) Å (Table 3), which are comparable to those in $Nd_2(MoO_4)(Te_4O_{10})$ and other neodymium tellurites reported.[14] Unlike that in $La_2(WO_4)(Te_3O_7)_2$, both of the W atoms in $Nd_2W_2Te_2O_{13}$ are octahedrally coordinated. W(1) is octahedrally coordinated by two O atoms from two tellurite groups and four terminal O atoms, whereas W(2) is octahedrally coordinated by one O atom from a tellurite group and five terminal O atoms. A pair of WO_6 octahedra are interconnected via edge-sharing (O(12)···O(13)) into a

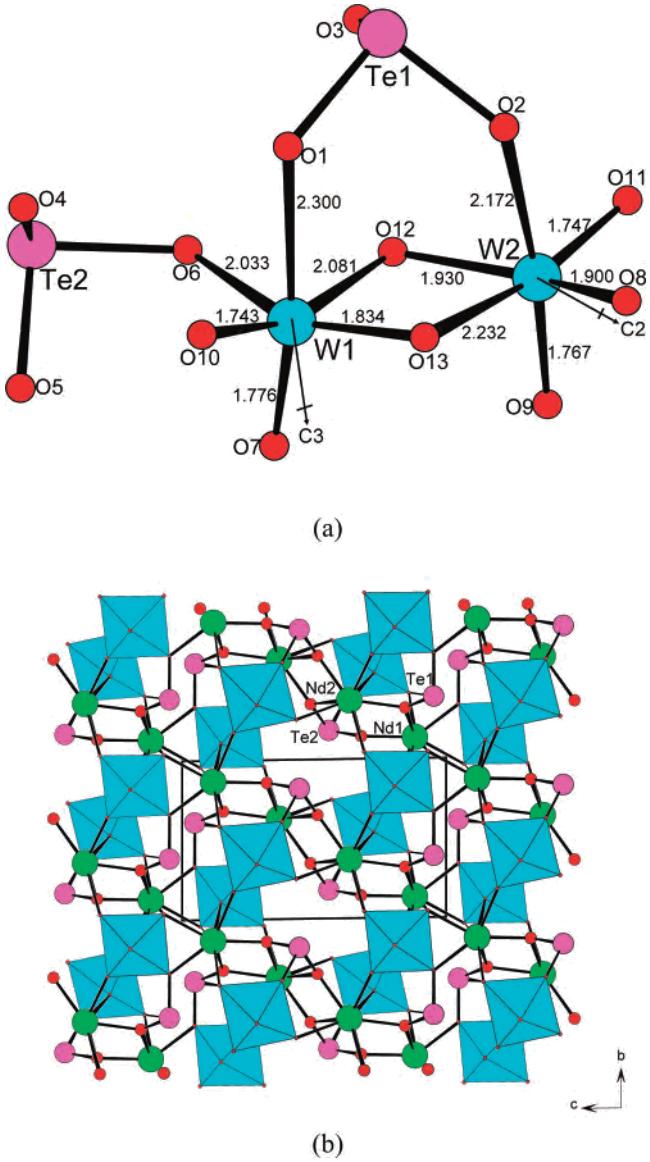

Figure 3. (a) $W_2Te_2O_{13}^{6-}$ anion in $Nd_2W_2Te_2O_{13}$. The directions of the distortions of the WO_6 octahedra are represented by arrows. (b) View of the structure of $Nd_2W_2Te_2O_{13}$ down the *a* axis. The WO_4 tetrahedra are shaded in cyan. Nd, Te, and O atoms are drawn as green, pink, and red circles, respectively.

$W_2O_{10}^{8-}$ dimer. Both of the WO_6 octahedra are severely distorted. The W−O bond distances are in the ranges of 1.743(6)−2.300(5) and 1.747(5)−2.232(5) Å respectively for W(1) and W(2) (Table 3). The O−W−O bond angles also deviate greatly from the ideal 90 and 180°, being in the ranges of 76.8(2)−168.0(2)° for $W(1)O_6$ and 72.5(2)−173.4(2)° for $W(2)O_6$. The W(1) atom is distorted toward a face formed by O(7), O(10), and O(13) atoms (local C_3 direction) with three short (1.743(6)−1.834(5) Å) and three long (2.033(5)−2.300(5) Å) W−O bonds (Table 3). The W(2) atom is distorted toward an edge (C_2) with two short (1.747(5) and 1.767(5) Å), two normal (1.900(5) and 1.930(5) Å), and two long (2.172(5) and 2.232(5) Å) W−O bonds (Figure 3a and Table 3).[3b] It is noticed that both W atoms are distorted away from the O atoms bonded to a Te^{4+} cation (Figure 3a), which is due to the distortion of the lone-pair electrons as well as the structural rigidity of the TeO_3 groups.[3b] Taking into account the six W−O bond lengths as well as the deviations from 180° of the three trans O−W−O bond angles, the magnitudes of the distortion (Δ_d) were calculated to be 1.118 and 0.945 Å respectively for $W(1)O_6$ and $W(2)O_6$; both are very strong ($\Delta_d > 0.80$ Å).[3b] The larger distortion of the $W(1)O_6$ octahedron can be attributed to the additional distortion-reinforcing TeO_3 group attached.[3b] Bond valence calculations indicate that the Mo atom is in an oxidation state of 6+ and the Te atoms are 4+; the calculated total bond valences for W(1), W(2), Te(1), and Te(2) are 6.11, 6.09, 3.95, and 3.95, respectively.[15]

Unlike those in $La_2(WO_4)(Te_3O_7)_2$, both tellurite groups ($Te(1)O_3$ and $Te(2)O_3$) in $Nd_2W_2Te_2O_{13}$ are discrete. The interconnection of the Nd(III) ions by the tellurite groups results in a 3D network with two types of apertures along the *a* axis (Figure 3b). The large apertures with a narrow-long shape are formed by 10-membered rings composed of four TeO_3 groups and six Nd atoms, and the small ones are formed by four-membered rings composed of two Nd(1) atoms and two $Te(1)O_3$ groups. The W_2O_{10} dimers are located at the large apertures (Figure 3b).

In $Nd_2W_2Te_2O_{13}$, each W_2O_{10} dimer connects with two TeO_3 groups, one in a unidentate fashion and the other in a bidentate bridging fashion, forming a $[W_2Te_2O_{13}]^{6-}$ anion (Figure 3a). Therefore, the structure of $Nd_2W_2Te_2O_{13}$ also can be viewed as the Nd^{3+} ions being interconnected by $[W_2Te_2O_{13}]^{6-}$ anions via Nd−O−Te and Nd−O−W bridges (Figure 3b).

When a Cl anion was introduced into the Ln−Mo(W)−Te−O system, $Ln_5(MO_4)(Te_5O_{13})(TeO_3)_2Cl_3$ (Ln = Pr, Nd; M = Mo, W) were obtained. The synthesis of $Ln_5(MO_4)(Te_5O_{13})(TeO_3)_2Cl_3$ (Ln = Pr, Nd; M = Mo, W) can be expressed by the following reaction at 710−730 °C: $Ln_2O_3 + 3LnOCl + MO_3 + 7TeO_2 \rightarrow Ln_5(MO_4)(Te_5O_{13})(TeO_3)_2Cl_3$. These four compounds are isostructural; hence, only the structure of $Nd_5(MoO_4)(Te_5O_{13})(TeO_3)_2Cl_3$ will be discussed in detail as a representative. The structure of $Nd_5(MoO_4)(Te_5O_{13})(TeO_3)_2Cl_3$ features a 3D network of neodymium(III) molybdenum tellurium oxychloride with large apertures occupied by isolated Cl anions and the lone-pair electrons of Te(IV) (Figure 4). The asymmetric unit of $Nd_5(MoO_4)(Te_5O_{13})(TeO_3)_2Cl_3$ contains three unique Nd(III), one Mo, and four Te atoms. Nd(1) at a site of C_2 symmetry is eight-coordinated by eight O atoms from six $Te_5O_{13}^{6-}$ groups, four of which are in a unidentate fashion and two of which are in a bidentate chelating fashion. Nd(2) is eight-coordinated by two O atoms from a $Te_5O_{13}^{6-}$ group, three O atoms from three $Te(4)O_3^{2-}$ anions, two terminal O^{2-} anions from two MoO_4^{2-} anions, and a Cl anion. Nd(3) is 10-coordinated by 10 O atoms from two $Te(4)O_3^{2-}$ anions and three $Te_5O_{13}^{6-}$ groups. The Nd−Cl distances (3.015(2) Å) are significantly longer than those of the Nd−O bonds (2.344(6)−2.937(8) Å) (Table 3). These bond distances are comparable to those reported for other neodymium tellurium(IV) oxides or oxyhalides.[14] The Mo atom occupying a site of the mirror plane is in a distorted tetrahedral coordination environment with Mo−O distances in the range of 1.714(10)−1.845(9) Å (Table 3). Te(1), Te(3), and Te(4) are three-coordinated by three O atoms in a distorted ψ-TeO_3 tetrahedral geometry with the fourth site occupied by the lone-pair electrons, whereas Te(2) is four-coordinated by four O atoms in a distorted ψ-TeO_4 tetragonal pyramidal geometry, with the lone pair of Te(IV) occupying the pyramidal site. $Te(1)O_3$ and $Te(2)O_4$ groups form a dimeric unit through corner-sharing, and two such dimers are further bridged by a $Te(3)O_3$ group into a novel $Te_5O_{13}^{6-}$ pentamer in a semicyclic shape. The Te−O distances fall in the range of 1.845(8)−2.162(6) Å, and the Te−O distances of the Te−O−Te bridge (1.899(7)−2.162(6) Å) are significantly longer than the remaining Te−O bonds (1.845(8)−1.889(6) Å) (Table 3). Results of bond valence calculations indicate that the Mo atom is in an oxidation state of 6+ and the Te atoms are 4+. The calculated total bond valences are 5.92, 3.73, 3.98, 3.81, and 3.94 respectively for Mo(1), Te(1), Te(2), Te(3), and Te(4).[15]

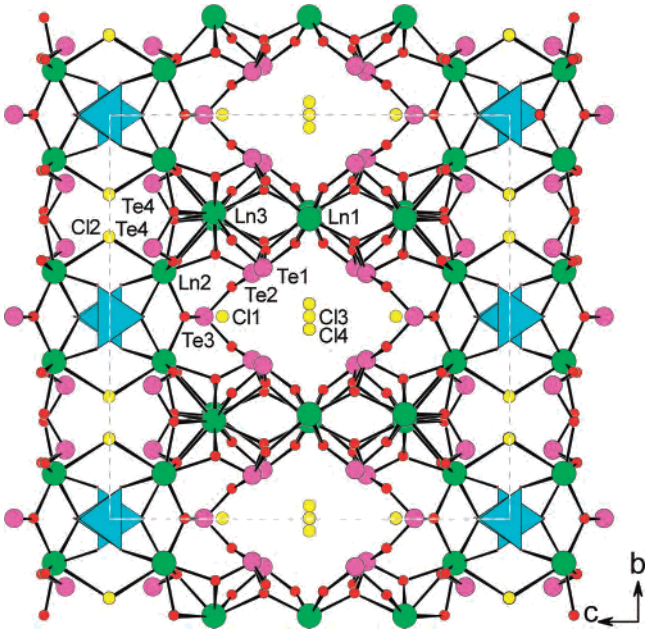

Figure 4. View of the structure of $Ln_5(MoO_4)(Te_5O_{13})(TeO_3)_2Cl_3$ down the *a* axis. The MoO_4 tetrahedra are shaded in cyan. Ln, Te, Cl, and O atoms are drawn as green, pink, yellow, and red circles, respectively.

The interconnection of Nd(III) ions via $Te_5O_{13}^{6-}$ and TeO_3^{2-} anions led to a thick double layer parallel to the *ab* plane. Neighboring neodymium(III) tellurium(IV) oxide layers are bridged by Cl(2) atoms into a complicated 3D network, forming two different types of apertures (Figure 4). The MoO_4 polyhedra located at the small apertures composed of $Nd_4O_2Cl_2$ rings are capping on both sides of the Nd_4 clusters. The isolated Cl anions and the lone-pair electrons of Te(IV) atoms of the $Te_5O_{13}^{6-}$ groups occupy the large apertures formed by eight-membered rings (two Nd(1) ions and two $Te_5O_{13}^{6-}$ anions, of which four TeO_3 groups are not involved in the ring formation). The size of the aperture is about 4.7 × 3.8 Å^2 based on structural data (the atomic radii of the ring atoms have been subtracted) (Figure 4).

Luminescent Properties. Under excitation at 448 nm, $La_2(WO_4)(Te_3O_7)_2$ displays a characteristic broad emission band at 489 nm for the WO_4^{2-} anion (Figure 5a).[18] The three Pr(III) compounds are capable of emitting luminescent light in the blue, green, and red regions. $Pr_5(MoO_4)(Te_5O_{13})(TeO_3)_2Cl_3$ and $Pr_5(WO_4)(Te_5O_{13})(TeO_3)_2Cl_3$ display four sets of emission bands at 491 nm (very strong, $^3P_0 \rightarrow {}^3H_4$), 534 nm (moderate, $^3P_0 \rightarrow {}^3H_5$), 619 nm (moderate, $^3P_0 \rightarrow {}^3H_6$), 649 nm (strong, $^3P_0 \rightarrow {}^3F_2$), and 735 nm (weak, $^3P_0 \rightarrow {}^3F_4$) under $\lambda_{ex} = 448$ nm (Figure 5b).[19] Under the same experimental conditions, the corresponding emission bands for $Pr_2(MoO_4)(Te_4O_{10})$ are much weaker (Figure 5b). Because of the so-called crystal field effect as well as multiple Pr^{3+} sites, a few transition bands of each have been split into several sub-bands (Figure 5b). The fewer sub-bands for $Pr_2(MoO_4)(Te_4O_{10})$ are due to fewer independent Pr^{3+} sites compared with those of $Pr_5(MO_4)(Te_5O_{13})(TeO_3)_2Cl_3$ (M = Mo, W). The solid-state luminescent properties of $Nd_5(MO_4)(Te_5O_{13})(TeO_3)_2Cl_3$ (M = Mo, W) were also investigated at room temperature. Under excitation at 514 nm, both of them display three sets of emission bands characteristic for the Nd(III) ion in the near-IR region: several emission bands at 870−923 nm ($^4F_{3/2} \rightarrow {}^4I_{9/2}$), a strong emission band at 1062−1069 nm ($^4F_{3/2} \rightarrow {}^4I_{11/2}$), and a weak band at about 1336−1345 nm ($^4F_{3/2} \rightarrow {}^4I_{13/2}$) in the near-IR region (Figure 5c).[11,20] The Nd ($^4F_{3/2}$) lifetime was measured to be 4.1 μs for $Nd_5(MoO_4)(Te_5O_{13})(TeO_3)_2Cl_3$ ($\lambda_{ex,em} = 514, 1068$). $Nd_2(MoO_4)(Te_4O_{10})$ and $Nd_2W_2Te_2O_{13}$ each contain two unique Nd(III) ions with C_1 symmetry, which are fewer than those for $Nd_5(MO_4)(Te_5O_{13})(TeO_3)_2Cl_3$ (M = Mo, W). Hence, it is worth investigating their solid-state luminescent properties at both room temperature and low temperature (10 K). Similar to $Nd_5(MoO_4)(Te_5O_{13})(TeO_3)_2Cl_3$ and $Nd_5(WO_4)(Te_5O_{13})(TeO_3)_2Cl_3$, $Nd_2(MoO_4)(Te_4O_{10})$ and $Nd_2W_2Te_2O_{13}$ display three sets of characteristic emission bands for the Nd(III) ion in the near-IR region (Figures 6 and 7 and Table 4) under excitation at 514 nm: $^4F_{3/2} \rightarrow {}^4I_{9/2}$, $^4F_{3/2} \rightarrow {}^4I_{11/2}$, and $^4F_{3/2} \rightarrow {}^4I_{13/2}$. As a result of the crystal field effect, each transition band was

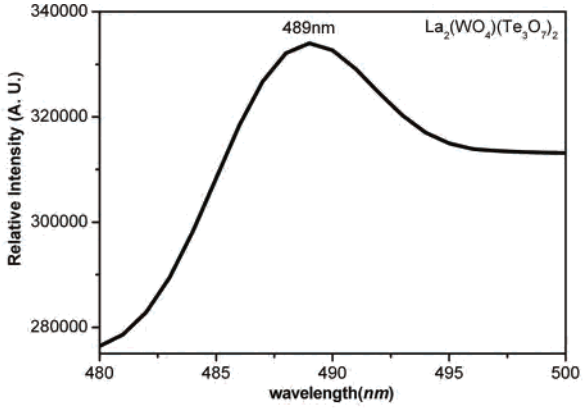

(a)

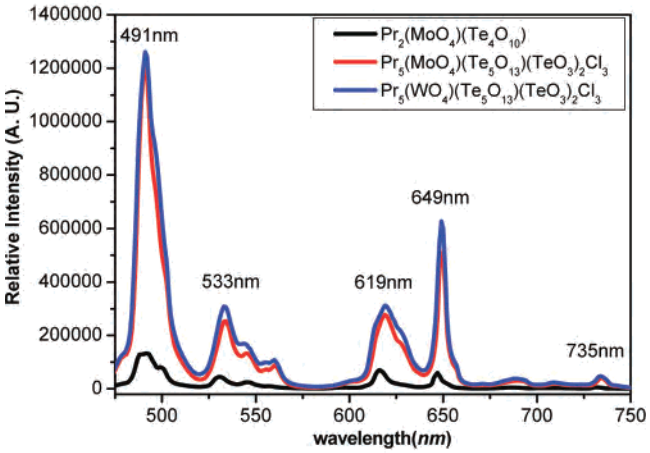

(b)

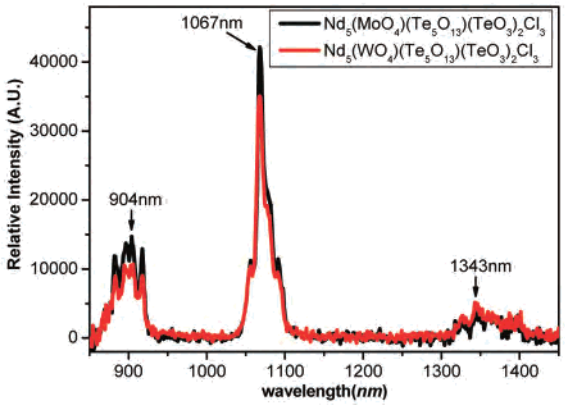

(c)

Figure 5. Solid-state emission spectra of $La_2(WO_4)(Te_3O_7)_2$ ($\lambda_{ex} = 448$ nm) (a), $Pr_2(MoO_4)(Te_4O_{10})$, $Pr_5(MoO_4)(Te_5O_{13})(TeO_3)_2Cl_3$, and $Pr_5(WO_4)(Te_5O_{13})(TeO_3)_2Cl_3$ ($\lambda_{ex} = 448$ nm) (b), and $Nd_5(MoO_4)(Te_5O_{13})(TeO_3)_2Cl_3$ and $Nd_5(WO_4)(Te_5O_{13})(TeO_3)_2Cl_3$ ($\lambda_{em} = 514$ nm) (c).

(18) Cho, W. S.; Yoshimura, M. *J. Appl. Phys.* **1998**, *83*, 518.
(19) Cybińska, J.; Hölsä, J.; Lastusaari, M.; Legendziewicz, J.; Meyer, G.; Wickleder, C. *J. Alloys Compd.* **2004**, *380*, 27.
(20) (a) Song, J. L.; Lei, C.; Mao, J. G. *Inorg. Chem.* **2004**, *43*, 5630. (b) Hebbink, G. A.; Grave, L.; Woldering, L. A.; Reinhoudt, D. N.; van Vegel, F. C. J. M. *J. Phys. Chem.* **2003**, *A107*, 2483. (c) Faulkner, S.; Pope, S. J. A. *J. Am. Chem. Soc.* **2003**, *125*, 10526. (d) Pope, S. J. A.; Kenwright, A. M.; Boote, V. A.; Faulkner, S. *J. Chem. Soc., Dalton Trans.* **2003**, 3780. (e) Wong, W. K.; Liang, H. Z.; Guo, J. P.; Wong, W. Y.; Lo, W. K.; Li, K. F.; Cheah, K. W.; Zhou, Z. Y.; Wong, W. T. *Eur. J. Inorg. Chem.* **2004**, 829.

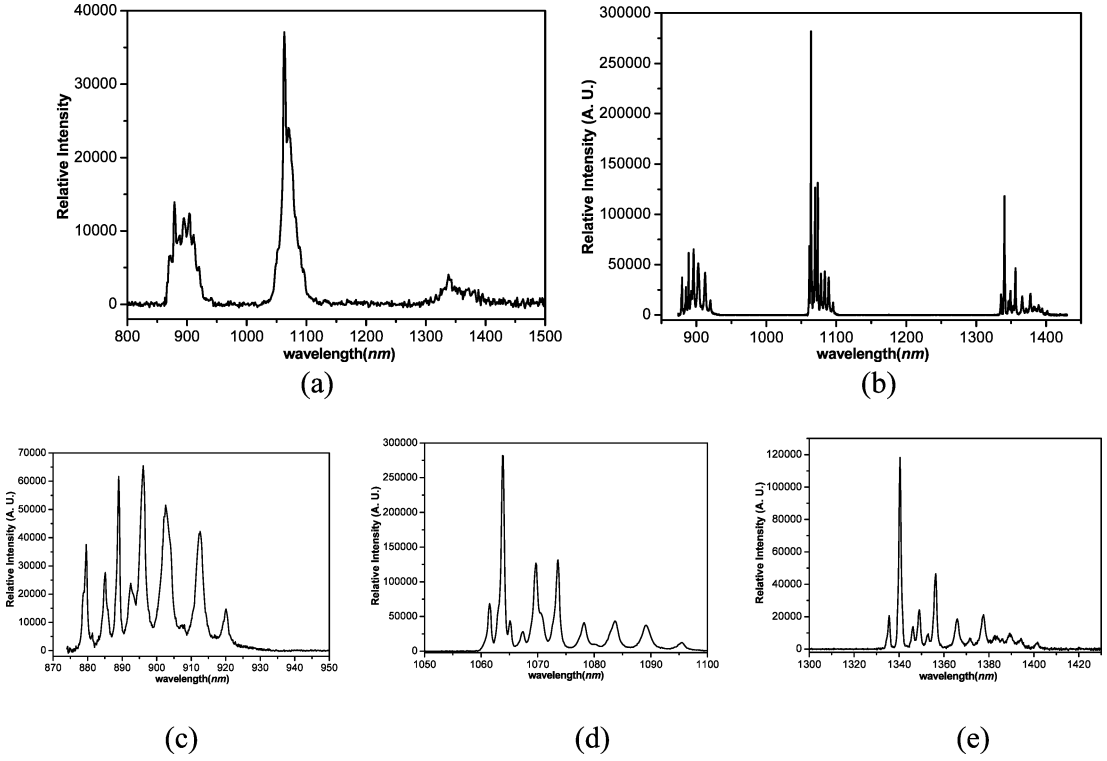

Figure 6. Solid-state emission spectra of $Nd_2(MoO_4)(Te_4O_{10})$ under excitation at $\lambda_{ex} = 514$ nm at room temperature (a), $\lambda_{ex} = 580$ nm at 10 K (b), and the enlarged emission bands for $^4F_{3/2} \rightarrow {}^4I_{9/2}$ (c), $^4F_{3/2} \rightarrow {}^4I_{11/2}$ (d), and $^4F_{3/2} \rightarrow {}^4I_{13/2}$ (e) transitions at 10 K.

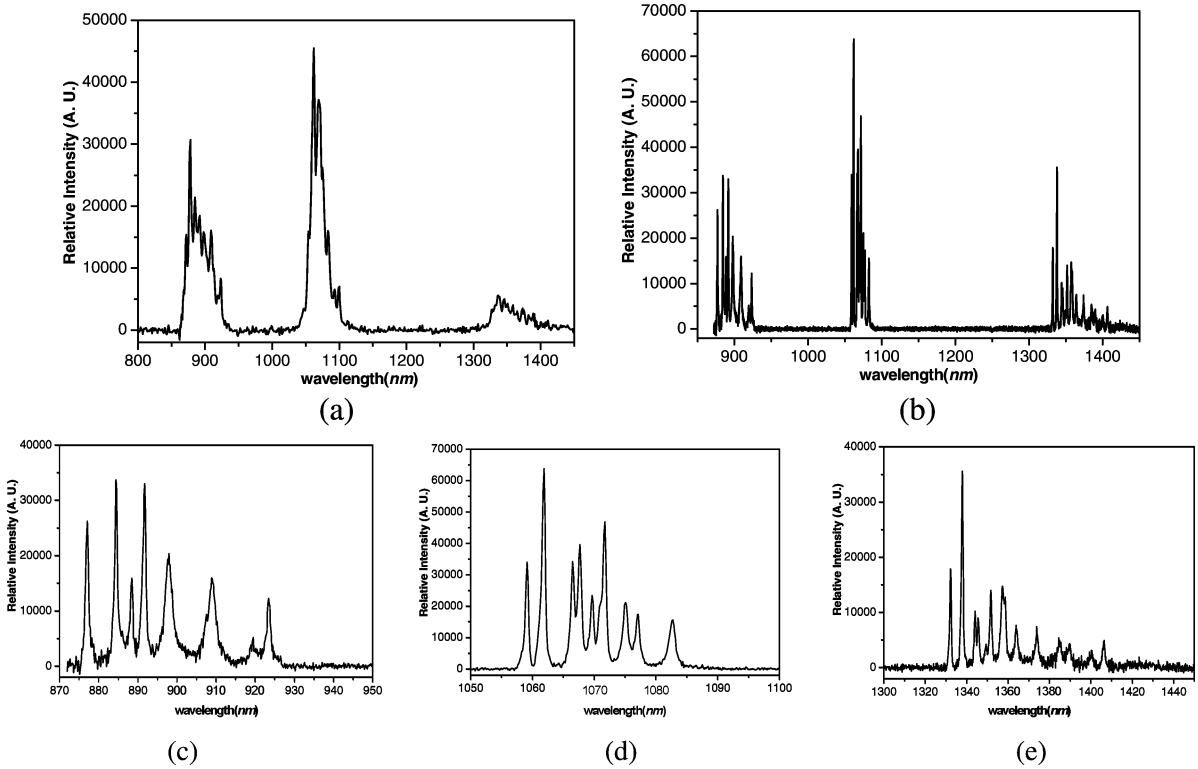

Figure 7. Solid-state emission spectra of $Nd_2W_2Te_2O_{10}$ under excitation at $\lambda_{ex} = 514$ nm at room temperature (a) and $\lambda_{ex} = 288$ nm at 10 K (b) and the enlarged emission bands for $^4F_{3/2} \rightarrow {}^4I_{9/2}$ (c), $^4F_{3/2} \rightarrow {}^4I_{11/2}$ (d), and $^4F_{3/2} \rightarrow {}^4I_{13/2}$ (e) transitions at 10 K.

split into several sub-bands (Table 4). The $^4F_{3/2}$ is expected to split into 2 sublevels, whereas the complete degeneracy of $^4I_{9/2}$, $^4I_{11/2}$, and $^4I_{13/2}$ leads to 5, 6, and 7 sublevels, respectively.[11] Therefore, $^4F_{3/2} \rightarrow {}^4I_{9/2}$, $^4F_{3/2} \rightarrow {}^4I_{11/2}$, and $^4F_{3/2} \rightarrow {}^4I_{13/2}$ transitions will have a maximum of 10, 12, and 14 sub-bands if both the lower and upper levels of $^4F_{3/2}$ are populated for a Nd(III) compound with one unique low-symmetric Nd(III) site. When two and more unique low-symmetric Nd(III) sites are present in a Nd(III) compound, its spectrum will be even more complicated. Because of the

Table 4. Observed Emission Bands (nm) for $Nd_2(MoO_4)(Te_4O_{10})$ and $Nd_2W_2Te_2O_{13}$ at Room Temperature and 10 K

	$Nd_2(MoO_4)(Te_4O_{10})$		$Nd_2W_2Te_2O_{13}$	
	RT	10 K	RT	10 K
$^4F_{3/2} \rightarrow {}^4I_{9/2}$	870.7, 878.6, 887.5, 894.5, 903.4, 910.9, 920.2	879.6, 885.1, 888.9, 892.5, 895.9, 902.6, 912.6, 920.0	871.6, 878.3, 884.9, 891.1, 898.1, 909.2, 923.3	877.2, 884.5, 888.7, 891.8, 897.7, 908.9, 919.5, 923.5
$^4F_{3/2} \rightarrow {}^4I_{11/2}$	1062.9, 1069.9	1061.5, 1063.8, 1065.2, 1067.3, 1069.7, 1073.6, 1078.2, 1083.7, 1089.2, 1095.6	1061.9, 1069.4, 1075.2, 1083.1, 1092.9, 1099.5	1059.2, 1061.8, 1066.5, 1067.7, 1069.7, 1071.7, 1075.1, 1077.1, 1082.6
$^4F_{3/2} \rightarrow {}^4I_{13/2}$	1338.0, 1343.1	1335.5, 1340.5, 1346.1, 1348.9, 1352.8, 1356.3, 1365.9, 1371.5, 1377.5, 1383.4, 1385.8, 1389.2, 1394.3, 1401.6	1336.5, 1345.8	1332.1, 1337.9, 1343.9, 1345.5, 1351.7, 1357.2, 1358.8, 1366.9, 1373.8, 1384.3, 1389.7, 1400.4, 1406.4

overlapping of some emission bands and the resolution limit of the instruments, the observed emission peaks at room temperature are usually much fewer than expected. At a very low temperature such as 10 K, the lower level of $^4F_{3/2}$ is the most populated, whereas the upper level is almost unpopulated; hence, the corresponding emission spectra have much better resolution (Figures 6 and 7). Because $Nd_2(MoO_4)(Te_4O_{10})$ and $Nd_2W_2Te_2O_{13}$ both contain two unique Nd sites with C_1 symmetry, it is expected that their emission spectra will display 10, 12, and 14 sub-bands for the $^4F_{3/2} \rightarrow {}^4I_{9/2}$, $^4F_{3/2} \rightarrow {}^4I_{11/2}$, and $^4F_{3/2} \rightarrow {}^4I_{13/2}$ transitions. Upon excitation at 580 nm, $Nd_2(MoO_4)(Te_4O_{10})$ displays 8, 10, and 14 sub-bands for the $^4F_{3/2} \rightarrow {}^4I_{9/2}$, $^4F_{3/2} \rightarrow {}^4I_{11/2}$, and $^4F_{3/2} \rightarrow {}^4I_{13/2}$ transitions at 10 K, whereas $Nd_2W_2Te_2O_{13}$ displays 8, 9, and 13 sub-bands for the $^4F_{3/2} \rightarrow {}^4I_{9/2}$, $^4F_{3/2} \rightarrow {}^4I_{11/2}$, and $^4F_{3/2} \rightarrow {}^4I_{13/2}$ transitions at 10 K upon excitation at 288 nm (Table 4 and Figures 6 and 7). Several sub-bands are not observed, probably because of the overlapping of two sets of transition bands for the two different Nd(III) sites. The lifetimes of $^4F_{3/2}$ were determined to be 3.2 and 3.6 μs for $Nd_2(MoO_4)(Te_4O_{10})$ ($\lambda_{ex,em}$ = 578, 1063) and $Nd_2W_2Te_2O_{13}$ ($\lambda_{ex,em}$ = 533, 1062), respectively.

Magnetic Properties. Magnetic properties for all of the compounds except for $La_2(WO_4)(Te_3O_7)_2$ have been studied at a magnetic field of 5000 Oe in the temperature range of 2−300 K. The plots of χ_m^{-1} versus temperature (T) are shown in Figure 8. $Pr_2(MoO_4)(Te_4O_{10})$ and $Nd_2(MoO_4)(Te_4O_{10})$ obey the Curie−Weiss law in the range of 50−300 K, whereas other compounds do above 75 K. At 300 K, the effective magnetic moments (μ_{eff}) are calculated to be 4.51 μ_B, 5.21 μ_B, 4.99 μ_B, 7.38 μ_B, 7.23 μ_B, 7.33 μ_B, and 7.73 μ_B respectively for $Pr_2(MoO_4)(Te_4O_{10})$, $Nd_2(MoO_4)(Te_4O_{10})$, $Nd_2W_2Te_2O_{13}$, $Pr_5(MoO_4)(Te_5O_{13})(TeO_3)_2Cl_3$, $Pr_5(WO_4)(Te_5O_{13})(TeO_3)_2Cl_3$, $Nd_5(MoO_4)(Te_5O_{13})(TeO_3)_2Cl_3$, and $Nd_5(WO_4)(Te_5O_{13})(TeO_3)_2Cl_3$, which are slightly smaller than the theoretical values (5.06 μ_B, 5.12 μ_B, 5.12 μ_B, 8.00 μ_B, 8.00 μ_B, 8.09 μ_B, and 8.09 μ_B, respectively). Upon cooling, the μ_{eff} values are decreased and reach 1.21 μ_B, 2.86 μ_B, 3.25 μ_B, 1.81 μ_B, 1.84 μ_B, 4.13 μ_B, and 4.12 μ_B at 2 K respectively for $Pr_2(MoO_4)(Te_4O_{10})$, $Nd_2(MoO_4)(Te_4O_{10})$, $Nd_2W_2Te_2O_{13}$, $Pr_5(MoO_4)(Te_5O_{13})(TeO_3)_2Cl_3$, $Pr_5(WO_4)(Te_5O_{13})(TeO_3)_2Cl_3$, $Nd_5(MoO_4)(Te_5O_{13})(TeO_3)_2Cl_3$, and $Nd_5(WO_4)(Te_5O_{13})(TeO_3)_2Cl_3$, indicating antiferromagnetic interactions between magnetic centers. Linear fitting of χ_m^{-1} data with T above 100 K gave Weiss constants of −34.1(1), −69.2(1), −43.4(3), −31.4(5), −30.6(3), −46.6(2), and −63.2(4) K respectively for $Pr_2(MoO_4)(Te_4O_{10})$, $Nd_2(MoO_4)(Te_4O_{10})$, $Nd_2W_2Te_2O_{13}$, $Pr_5(MoO_4)(Te_5O_{13})(TeO_3)_2Cl_3$, $Pr_5(WO_4)(Te_5O_{13})(TeO_3)_2Cl_3$, $Nd_5(MoO_4)(Te_5O_{13})(TeO_3)_2Cl_3$, and $Nd_5(WO_4)(Te_5O_{13})(TeO_3)_2Cl_3$. It should be noted that the Weiss constants for Nd(III) compounds are much more negative than those of the corresponding Pr(III) compounds. Because Mo(VI), W(VI), TeO_3^{2-}, $Te_4O_{10}^{4-}$, and $Te_5O_{13}^{6-}$ are diamagnetic, the paramagnetic contributions are expected to come solely from the Ln^{3+} ions. The shortest Ln···Ln separations are 3.9699(8) Å for $Pr_2(MoO_4)(Te_4O_{10})$, 3.9307(8) Å for $Nd_2(MoO_4)(Te_4O_{10})$, 3.9341(13) Å for $Nd_2W_2Te_2O_{13}$, 3.8337(8) Å for $Pr_5(MoO_4)(Te_5O_{13})(TeO_3)_2Cl_3$, 3.8503(11) Å for $Pr_5(WO_4)(Te_5O_{13})(TeO_3)_2Cl_3$, 3.8308(4) Å for $Nd_5(MoO_4)(Te_5O_{13})(TeO_3)_2Cl_3$, and 3.82762(16) Å for $Nd_5(WO_4)(Te_5O_{13})(TeO_3)_2Cl_3$. These data could explain most of the Weiss constants observed. More detailed calculations of these magnetic interactions were not performed because of the complexity of the structures as well as the lack of suitable models.

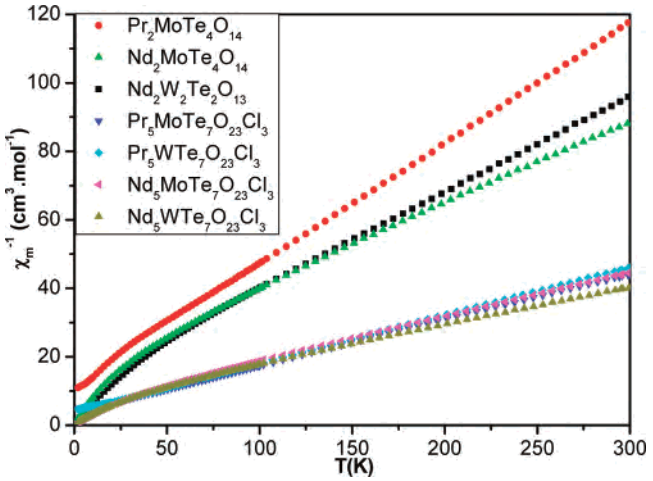

Figure 8. Plots of χ_m^{-1} versus temperature (T) for $Pr_2(MoO_4)(Te_4O_{10})$, $Nd_2(MoO_4)(Te_4O_{10})$, $Nd_2W_2Te_2O_{13}$, $Pr_5(MoO_4)(Te_5O_{13})(TeO_3)_2Cl_3$, $Pr_5(WO_4)(Te_5O_{13})(TeO_3)_2Cl_3$, $Nd_5(MoO_4)(Te_5O_{13})(TeO_3)_2Cl_3$, and $Nd_5(WO_4)(Te_5O_{13})(TeO_3)_2Cl_3$.

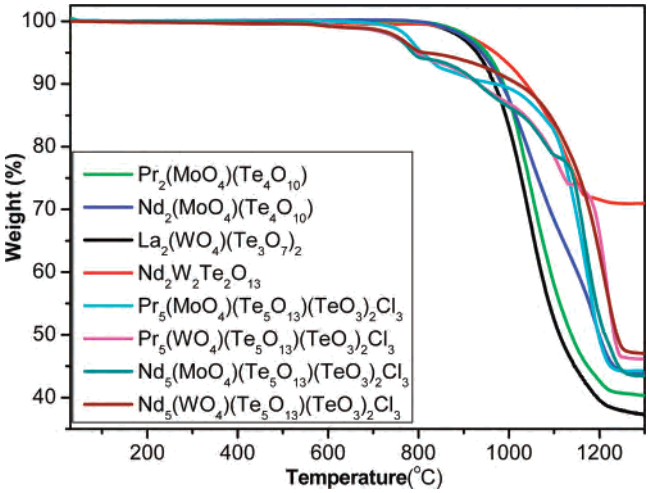

Figure 9. TGA curves for $Pr_2(MoO_4)(Te_4O_{10})$, $Nd_2(MoO_4)(Te_4O_{10})$, $La_2(WO_4)(Te_3O_7)_2$, $Nd_2W_2Te_2O_{13}$, $Pr_5(MoO_4)(Te_5O_{13})(TeO_3)_2Cl_3$, $Pr_5(WO_4)(Te_5O_{13})(TeO_3)_2Cl_3$, $Nd_5(MoO_4)(Te_5O_{13})(TeO_3)_2Cl_3$, and $Nd_5(WO_4)(Te_5O_{13})(TeO_3)_2Cl_3$.

TGA Analysis. TGA analyses under an oxygen atmosphere indicate that these compounds are stable up to 770 °C (for $Pr_2(MoO_4)(Te_4O_{10})$), 770 °C (for $Nd_2(MoO_4)(Te_4O_{10})$), 800 °C (for $La_2(WO_4)(Te_3O_7)_2$), 810 °C (for $Nd_2W_2Te_2O_{13}$), 554 °C (for $Pr_5(MoO_4)(Te_5O_{13})(TeO_3)_2Cl_3$), 550 °C (for $Pr_5(WO_4)(Te_5O_{13})(TeO_3)_2Cl_3$), 544 °C (for $Nd_5(MoO_4)(Te_5O_{13})(TeO_3)_2Cl_3$), and 557 °C (for $Nd_5(WO_4)(Te_5O_{13})(TeO_3)_2Cl_3$) (Figure 9). $Pr_2(MoO_4)(Te_4O_{10})$, $Nd_2(MoO_4)(Te_4O_{10})$, $La_2(WO_4)(Te_3O_7)_2$, and $Nd_2W_2Te_2O_{13}$ are thermally much more stable than the four chloride-containing phases, which could be attributed to some isolated chloride ions present in the latter four phases and the fact that Ln−O bonds are normally much stronger than Ln−Cl bonds. $Pr_2(MoO_4)(Te_4O_{10})$, $Nd_2(MoO_4)(Te_4O_{10})$, $La_2(WO_4)(Te_3O_7)_2$, and $Nd_2W_2Te_2O_{13}$ only exhibit one main step of weight loss, which corresponds to the release of TeO_2. $Pr_5(MoO_4)(Te_5O_{13})(TeO_3)_2Cl_3$, $Pr_5(WO_4)(Te_5O_{13})(TeO_3)_2Cl_3$, $Nd_5(MoO_4)(Te_5O_{13})(TeO_3)_2Cl_3$, and $Nd_5(WO_4)(Te_5O_{13})(TeO_3)_2Cl_3$ display two main steps of weight losses. The first one is the release of Cl_2, and the second one corresponds to the loss of TeO_2. The total weight losses at 1300 °C are 58.7%, 56.7%, 28.6%, 55.7%, 53.8%, 56.4%, 52.9%, and 63.2% respectively for $Pr_2(MoO_4)(Te_4O_{10})$, $Nd_2(MoO_4)(Te_4O_{10})$, $Nd_2W_2Te_2O_{13}$, $Pr_5(MoO_4)(Te_5O_{13})(TeO_3)_2Cl_3$, $Pr_5(WO_4)(Te_5O_{13})(TeO_3)_2Cl_3$, $Nd_5(MoO_4)(Te_5O_{13})(TeO_3)_2Cl_3$, $Nd_5(WO_4)(Te_5O_{13})(TeO_3)_2Cl_3$, and $La_2(WO_4)(Te_3O_7)_2$. The final residues were not characterized because of their melting with the TGA buckets made of Al_2O_3 under such high temperature.

Conclusion

In summary, the syntheses, crystal structures, and luminescent properties of eight new rare-earth tellurite oxides or oxyhalides containing additional $Mo(W)O_4$ tetrahedra or WO_6 octahedra have been reported. Their structures can be viewed as lanthanide tellurium(VI) oxide/oxyhalide-based open frameworks being decorated with $Mo(W)O_4$ tetrahedra or WO_6 octahedra. The $Mo(W)O_6$ octahedra are severely distorted, whereas the $Mo(W)O_4$ tetrahedra are only slightly distorted. Several new polymeric tellurium(IV) oxide anions are discovered: the 1D $Te_4O_{10}^{4-}$ anion in $Ln_2(MoO_4)(Te_4O_{10})$ (Ln = Pr, Nd), the layered $Te_6O_{14}^{4-}$ layer in $La_2(WO_4)(Te_3O_7)_2$, and the $Te_5O_{13}^{6-}$ pentamer in $Ln_5(MO_4)(Te_5O_{13})(TeO_3)_2Cl_3$ (Ln = Pr, Nd; M = Mo, W). It is interesting to note that the three Pr(III) compounds can emit blue, green, and red light, whereas the four Nd(III) phases display strong emission bands in the near-IR region. All of these compounds have a high thermal stability and display strong luminescence; hence, they are possible candidates for luminescent materials in laser or luminescence devices. It is anticipated that many other new compounds with novel structures and luminescent properties can be discovered in similar systems.

Acknowledgment. This work was supported by National Natural Science Foundation of China (Grants 20573113, 20371047, and 20521101), NSF of Fujian Province (Grant E0420003), and Key Project of CAS (Grant KJCX2-YW-H01). We thank Dr. Gang Xu for his great help with the luminescent measurements of La and Pr compounds.

Supporting Information Available: X-ray crystallographic files in CIF format, simulated and experimental powder XRD patterns, and χ versus T and χ^{-1} versus T plots. These materials are available free of charge via the Internet at http://pubs.acs.org.

IC700793N